Titania-based photocatalytic coatings on stainless steel hospital fixtures

S. Krumdieck[1*], S. S. Miya[1], D. Lee[2], S. Davies-Talwar[2], C.M. Bishop[1]

1 Department of Mechanical Engineering, Private Bag 4800, University of Canterbury, Christchurch, 8041, New Zealand.
2 Koti Technologies, Inc., PO Box 29519, Christchurch, 8041, New Zealand.

Received ZZZ, revised ZZZ, accepted ZZZ
Published online ZZZ (Dates will be provided by the publisher.)

Keywords photocatalytic, TiO2, pp-MOCVD, processing

A scaled-up pulsed-pressure MOCVD system was used to deposit TiO_2 coatings from tetra-isopropoxide precursor solution on stainless steel substrates and on 3-D objects. The objective of the work is the production of antimicrobial coatings for handles in health care facilities. Antimicrobial coatings are sought to manage the transmission of hospital acquired infections (HAI's), which are reported to cost around one million pounds per annum in the UK alone. Titania is a promising material for this application due to the photocatalytic production of reactive oxygen species that are crucial for the destruction of organic pathogens.

TiO_2 coatings of 0.2 to 13 μm thickness were deposited at temperatures between 375 ^oC and 475 ^oC. The crystallite size and photocatalytic activity are influenced by deposition temperature. No dependence of stoichiometry on the deposition temperature has been observed. The films on stainless steel exhibit reasonably good photocatalytic performance. The photocatalytic performance and the stoichiometry improve with the film thickness. A three dimensional object (door handle) was coated with good conformity. The reactor scale-up for coating production on door handles is proposed for future wear and hygiene performance testing.

1 Introduction

1.1 Antimicrobial materials More than five decades ago contaminated touch surfaces were first incriminated in transmission of diseases [1]. The transmission of diseases can lead to hospital acquired infections (HAIs) defined as infections neither detected nor incubating when patients are admitted to hospitals. The consequences of HAIs include prolonged hospital stays that are accompanied by advanced morbidity and increased mortality [2, 3]. It is reported that 9.0 percent of patients contract HAIs in the UK and the Republic of Ireland hospitals [3]. The United Kingdom's National Health Services estimated the costs related to HAIs to be around one million pounds per annum [2].

The current approach to reducing the prevalence of HAI's relies on cleaning, including hands hygiene, and deep cleaning of inanimate surfaces [4, 5]. Antifouling, anti-adhesive and anti-microbial (AM) coatings on "high touch" inanimate surfaces are currently being pursued as a complimentary strategy for reducing transmission of HAI's [6]. These methods are faced with challenges that hinder their effectiveness [4, 5, 6]. The main issues with current cleaning chemicals are the harshness and exposure for workers and the growing resistance to antimicrobial agents by bacteria. The main issues for coating materials on touch surfaces are adhesion and wear. If an antifouling coating cracks, blisters or peels, it can actually increase the contamination potential by creating hard-to-clean areas that can harbor microbes.

Research is now focusing on finding wear-resistant antimicrobial materials and testing them for efficacy against the antibiotic resistant "superbug" bacteria mainly MRSA and MRSE. [7]. Elemental silver and copper are well known antimicrobial materials that work by poisoning cells once metal ions cross the cell wall. Some studies have reported on silver and silver ions exhibiting almost the same antibacterial activities [8]. Recently it has been reported that the pure silver nanoparticles have no AM activity, and that the lethality to microbes is dependent on and highly sensitive to the reducing agent in an aqueous solution [9]. The vast majority of research reports are focused on the processing methods and materials characterization of copper and silver composites, alloys, nanotubes, and nanoparticles, and not on the effectiveness in use as touch-surfaces, the manufacturing of coated parts, adhesion or wear properties. Open questions exist around the wear of bio-toxic nano-particles, their life, and the eventual impacts they may have on the environment [10].

1.2 TiO_2 antifouling and photocatalytic activity Titanium dioxide (TiO_2) causes cell death by direct oxidation. TiO_2 was first reported to exhibit photocatalytic (PC) behaviour when it was used for the splitting of water under ultraviolet illumination in 1972 [11]. Titania is non-toxic and has high chemical and thermal stability [12]. The interaction of TiO_2 with light with wavelengths of 388 nm or below leads to the excitation of carriers which then oxidize and/or reduce water and oxygen molecules adsorbed onto the surface. The redox reactions taking place on the TiO_2 surface lead to the formation of reactive oxygen species (superoxides and hydroxly radicals) [11]. The nonselective hydroxyl radicals have been reported to be key in the destruction of pathogens [6]. TiO_2 exists in three stable phases at atmospheric pressure: anatase, rutile and brookite. The three phases preferentially deposit in CVD at different temperatures. The most important phase for photocatalysis applications is anatase [13]. Anatase TiO_2 has been of high interest for a number of years as a waste treatment catalyst, self-cleaning surface and as an AM coating.

Plasma spray, powder coating and paint are the current available methods to apply TiO_2 to metal objects [14]. It is not known if TiO_2 applied by these methods has PC activity. Current self-cleaning TiO_2 coatings are applied to glass by atmospheric pressure MOCVD using titanium isopropoxide (TTIP) [15]. There are no MOCVD processes reported in the literature or available in industry currently applying thick (>10 μm) TiO_2 coatings to complex shaped metal parts.

1.3 Effect of TiO_2 Phase and Morphology on PC activity TiO_2 anatase phase is the most PC active phase. This has been attributed to a longer life-time and a higher mobility of excited carriers that lead to much longer diffusion lengths in this phase than in the rutile phase [16]. The higher activity of the anatase phase has also been attributed to higher localised states density which leads to a higher density of surface-adsorbed hydroxyl radicals and reduced recombination in this phase. The PC activity can also be improved by mixing the two phases (80% anatase and 20% rutile) due to charge carrier separation attained as a result of confinement of photoexcited carriers in the different phases which leads to reduced recombination. The surface roughness has been reported to have a negligible effect on the PC activity of single crystalline rutile TiO_2 [17]. According to Hernandez-Alonso *et al.* [18] an increase in the surface area of the photocatalyst is accompanied by an increase in the probability of formation of lattice defects. This situation can however be avoided by synthesizing mono-dispersed nanoparticles that present an optimal diameter for which the benefits of small crystallite size supersedes the detrimental effects [18]. The importance of the crystallite size can also be explained in terms of the surface area of the photocatalyst. Smaller crystallites yield a higher number of active sites [19].

1.4 Effect of MOCVD TiO_2 coating thickness on PC activity Low growth rates and long deposition times in atmospheric pressure MOCVD of TiO_2 have been reported to lead to a cross contamination between the coatings and stainless steel (SS) substrates (the film's cations diffuse into the metal and the Fe^{3+} and Cr^{3+} cations from the passive SS oxide layer diffuse into the coating). The diffusion of ions from the SS passive oxide layer has been reported to favour nucleation of the less desirable rutile phase in films of less than 100 nm. However, after a complete coverage of the substrate with rutile TiO_2 nucleation of anatase TiO_2 begins. As the thickness of the coating increases more anatase TiO_2 starts to form and this leads to an increase in the PC activity [20]. An increase in the thickness of TiO_2 coatings has also been reported to reduce the influence of lattice imperfections (caused by Fe and Cr cations) at and/or close to the coating/substrate interface. Lattice imperfections may lead to carrier scattering and recombination [21].

1.5 Objectives of this research This study presents results on pulsed pressure metal-organic vapour deposition (pp-MOCVD) of TiO_2 films on SS substrates. SS is the most common material for "high touch surfaces" (bed rails, lift push buttons and door handles) at healthcare facilities. pp-MOCVD is cost effective and has the potential to produce uniform coatings on a manufacturing scale [22]. Dependence of the properties of the films on the deposition temperature and nominal film thickness were investigated. The properties studied include the microstructure, stoichiometry, crystal structure and the PC activity. We also demonstrate uniform coating of a complex-shaped object, a door handle, with a thick TiO_2 coating.

2 Methods

2.1 Pulsed-Pressure MOCVD Process

The basic operating principle of the pp-MOCVD process is timed liquid injection through an ultrasonic atomizer into a continuously evacuated cold-wall reactor, with no carrier gas flow. This operation results in rapid and extreme pressure rise in the reactor when the atomized liquid flash evaporates. At the peak of the pressure pulse, the maximum processing pressure is reached, and the flow conditions in the reactor are quiescent and well-mixed with uniform temperature and concentration fields [23]. The reactor size is important in determining the optimal concentration of precursor in solution and the precursor solution injection volume. The reactor is then pumped down, but the rate of precursor vapor diffusion through the reactor is much faster than the vacuum pumping rate, resulting in potentially high precursor conversion efficiency [24]. We have previously described TiO_2 deposition from titanium tetra-iso-propoxide $Ti(OC_3H_7)_4$ (TTIP) in toluene solvent [25, 26]. In this research we use the precursor concentration, deposition temperatures, pulse timing and precursor solution injection volume identified in previous studies.

The pp-MOCVD apparatus used in this study is a scaled-up system with custom formed induction coil heater designed for larger substrates with complex geometries [24]. Figure 1 illustrates the reaction chamber with injection nozzle in the center base, holders for 8 door handles heated by induction coil. The reactor chamber has volume of approximately 14.7 litres and uses liquid injection of 250 µL at 8 s intervals with pump-down to 75 Pa. The concentration of TTIP in toluene was 5 mol%.

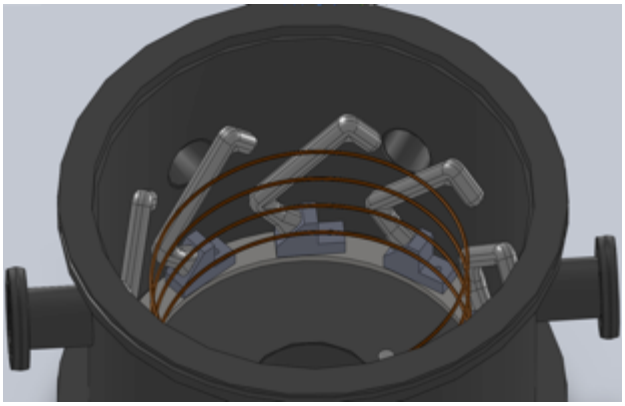

Figure 1 pp-MOCVD reaction chamber with door handles ready for titania deposition.

The substrates used for deposition of TiO_2 coatings were 30 mm x 30 mm x 5 mm AISI 304L SS plates. The substrates were degreased with ethanol and ultrasonically cleaned in a bath of water and detergent solution. Each substrate was placed on borosilicate glass holders and heated using a RF induction coil heater during the deposition. Coatings with different thickness were deposited at the same temperature by varying the number of pulses. Growth rates at 400 ^oC were 0.32 µm/min. Table 1 gives the deposition conditions and thickness measured with surface profilometer.

Table 1 Deposition parameters for TiO_2 coatings on SS substrates with measured thickness.

ID	Temperature (°C)	Number of Pulses	Measured Coating Thickness (µm)
2	400	300	12.60
3	400	150	6.30
4	400	30	1.26
5	400	15	0.63
6	400	4	0.17
7	375	305	6.43
8	425	290	5.49
9	450	290	7.29
10	475	295	7.23

2.4 Analytical Methods A SuperNova, Dual, Cu at zero, Atlas diffractometer using Cu K_α (λ = 0.15418 nm) radiation was used to study the phase of the films. The angle between the incident X-ray beam (collimated to a diameter of 0.3 mm) and the samples was fixed at 15^o while the detector was rotated at angles between 0^o and 80^o. A JEOL 7000F field emission scanning electron microscope (FE-SEM) was used to image the microstructure. A JOEL 6100 SEM equipped with an Oxford EXL energy dispersive x-ray analysis system was used for energy dispersive spectroscopy (EDS) to determine the composition of the films. A TiO_2 standard was used to optimise the imaging parameters and in provide a standard for oxygen to titanium ratio (O:Ti) of 2. An accelerating voltage of 10 kV was found to be suitable to give this O:Ti ratio.

The photocatalytic (PC) activity was assessed by the time of degradation of dye under UV light exposure as indicated by colour change of the dye. The measurement system consists of an irradiation cell with 200 W/m^2 UVA light with wavelength 365 nm. The radiation level was approximately four times summer sunlight. The RZ PC test ink and Kbar ink applicator from Queens University Belfast were used to spread an even coat of ink on the coated surface [27, 28]. A camera with timer was used to observe the colour change of the dye from blue to pink then clear due to photocatalytic activity of the dry TiO_2 surface. An image-based RGB extraction system enabled semi-quantitative analysis of the PC activity.

3 Results and Discussion

3.1 Coating quality Figure 2 shows the samples with coatings deposited at the same temperature (400 ^oC) with a varying number of pulses resulting in different thicknesses. The colour of the coating surface changes from the shiny bare SS substrate to dull grey. Due to thermal gradients from the induction heating, the coatings are thicker at the outer edges, hence the observable iridescences.

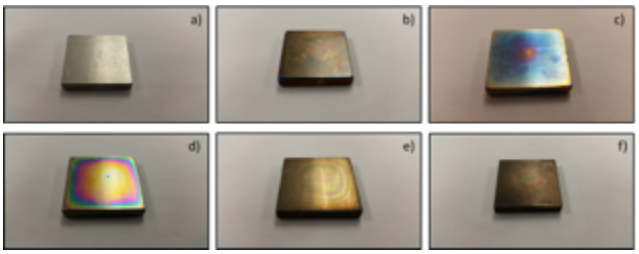

Figure 2 TiO_2 coatings deposited at 400 ^oC on 30x30mm SS substrates with coating thicknesses of; a) uncoated, b) 0.68 µm c) 0.63 µm, d) 1.26 µm, e) 6.43 µm, f) 12.60 µm.

SEM images of coatings corresponding to the samples in Figure 2 are shown in Figure 3. The SEM images of the surface of the coatings show typical TiO_2 morphology such as observed by Kajitvichyanukul and Amorncha [29] for TiO_2 prepared by sol-gel methods on stainless steel. The surface micrographs show the main features related to the SS surface, with coatings becoming visible for thickness over 5 µm.

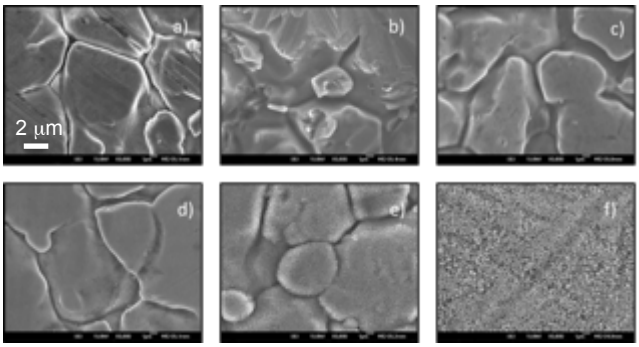

Figure 3 SEM images (all at X5,000 magnification) of surface morphology of samples; a) uncoated SS and coated with TiO_2 at 400 ^oC to achieve nominal coating thicknesses of b) 0.17 μm c) 0.63 μm d) 1.26 μm e) 6.30 μm and f) 12.60 μm.

Figure 4 shows coatings with nominal thickness of 6 μm deposited at varying temperatures (from 375 ^oC to 475 ^oC). All coating surfaces look similar to each other with light colour bands still visible except for the one deposited at the highest temperature of 475 ^oC. This particular coating shows a darker shade of grey and delamination is clearly visible on the bottom edge and corners in Figure 4 f).

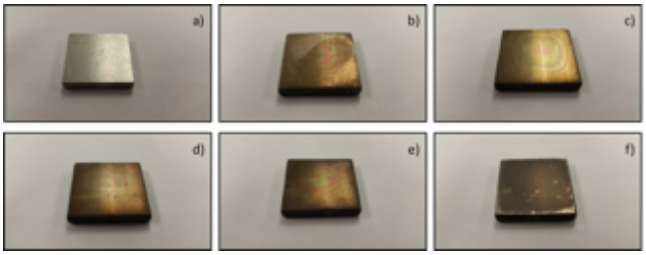

Figure 4 30x30mm stainless steel substrates coated with TiO_2 with different number of pulses to achieve nominally ≈ 6 μm thick coatings at different temperatures; a) uncoated, b) 375 ^oC, c) 400 ^oC, d) 425 ^oC, e) 450 ^oC and f) 475 ^oC.

Figure 5 shows SEM images of TiO_2 coatings in Figure 4 deposited at varying temperatures with nominal thicknesses of ≈ 6.0 μm.

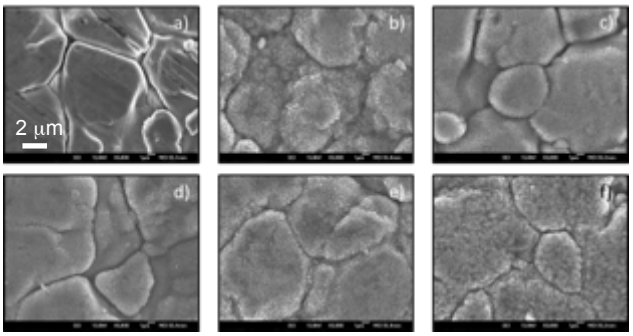

Figure 5 SEM images (all at X5,000 magnification) of surface morphology of nominally ≈ 6.00 μm thick TiO_2 films deposited at a range of temperatures; a) uncoated SS, b) 375 ^oC, c) 400 ^oC, d) 425 ^oC, e) 450 ^oC and f) 475 ^oC.

Figure 6 is a higher magnification SEM image showing the morphology of the surface of a coating deposited at 475 ^oC. The crystalline morphology is typical of all of the coatings produced on the stainless steel over all the temperatures in the range of the study. The morphology is also consistent with previously produced polycrystalline titania films on silicon where the grains are columnar anatase and mixed anatase and rutile [26]. Average surface crystal size was determined from surface SEM images.

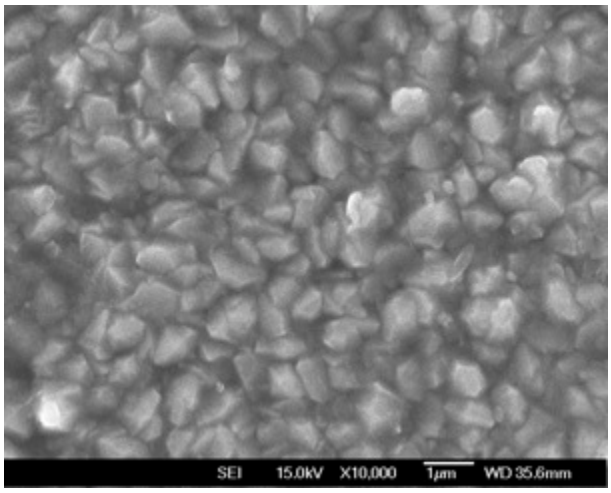

Figure 6 Surface SEM image of a typical coating with a thickness of 7.23 μm deposited at 475 ^oC.

Mean crystallite size (diameter) was determined from surface SEM images like Figure 6 using the circle intercept method [30]. Figure 7 shows that the mean crystallite size has a minimum at 400 ^oC and increases with increasing deposition temperature, as expected from previous studies [26].

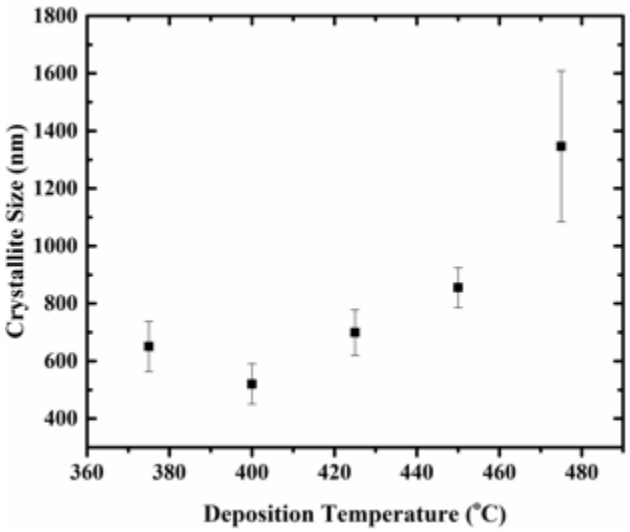

Figure 7 Dependence of crystallite size on deposition temperature.

Increasing crystallite size with increasing deposition temperature has been observed for atomic layer deposited TiO_2 coatings on silicon substrates and has been attributed to the composite effect of nucleus density and grain coalescence with temperature [31]. According to Cheng and Chen [31], increasing the deposition temperature yields a higher subsequent crystallite nucleation and coalescence resulting in a coarser crystallite size.

Figure 8 gives the EDS measurements of the O:Ti ratio and the presence of iron in the films deposited over a range of temperatures but having the same thickness. The O:Ti ratio is not strongly dependent on the deposition temperature. All the coatings deposited at varying temperatures are slightly oxygen deficient except for the one deposited at 400 °C with a O:Ti of 2.0. The average O:Ti ratio for the rest of the samples is 1.8. Lee et al. [32] observed a deficiency of oxygen in MOCVD TiO_2 deposited below 550 °C. And they attributed this to a lack of reaction between Ti atoms and oxygen atoms at low temperatures. Figure 8 indicates an increase in the amount of Fe detected with increasing in deposition temperature.

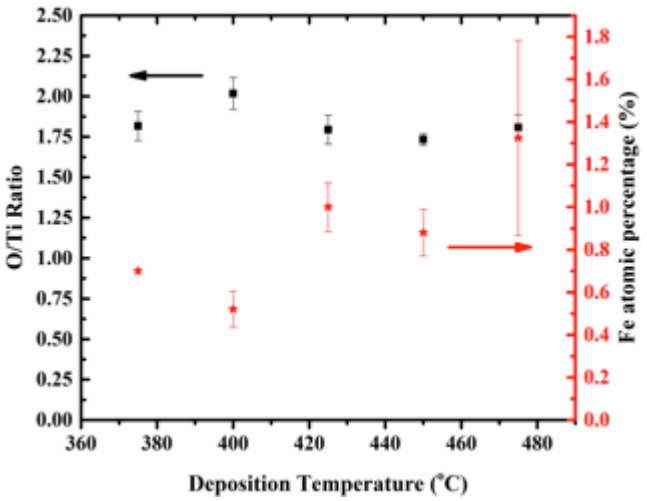

Figure 8 O:Ti atomic ratio and Fe concentration measured by EDS for TiO_2 coatings deposited at a range of temperatures with nominal 6 μm thickness. Error bars are the standard deviation over five measurements.

Figure 9 shows the dependence of the O:Ti ratio and the Fe and Cr atomic percentage on the coating thickness. Measurements for samples with nominal coating thicknesses less than 5 μm indicated the presence of Cr. As the surface of the SS has a native Cr-rich oxide, these measurements include information about the substrates and the atomic percentages of elements that cannot be extracted without using a layered model. The O:Ti ratio can be interpreted for the thickest coatings which are stoichiometric or slightly oxygen deficient. This phenomenon can be explained in terms of the diffusivity of the Fe and Cr in TiO_2. Fe has a relatively high diffusivity in rutile TiO_2 compared to other metals [33] and is detected in all of the 6 μm coatings, but at concentration less than 1.5 atomic percent. The Fe concentration increases with deposition temperature (shown in Figure 8). This is as expected if the incorporation in the film is controlled by diffusivity which increases with temperature. Since all coatings were made in about the same time, the diffusivity seems to be the determining factor.

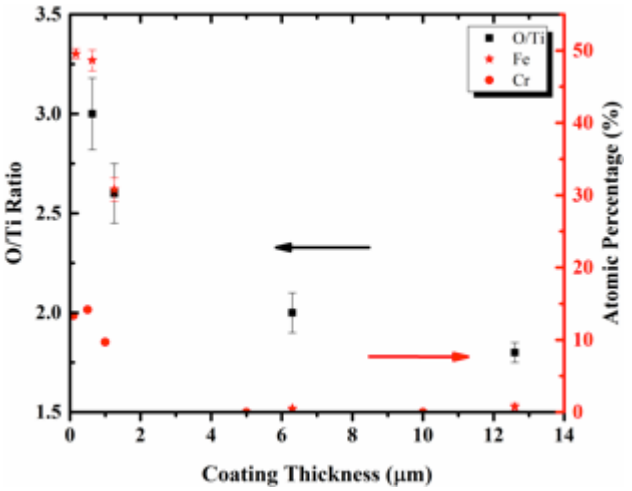

Figure 9 O:Ti atomic ratio and Fe and Cr concentration measured by EDS in TiO_2 coatings deposited at 400 °C with a range of thicknesses. Error bars are the standard deviation over five measurements.

3.2 Phase and Crystal Structure Figure 10 shows XRD spectra of three samples and an uncoated piece of SS. The coatings have thicknesses of 12.6 μm, 6.30 μm and 0.63 μm and were all deposited at 400 °C.

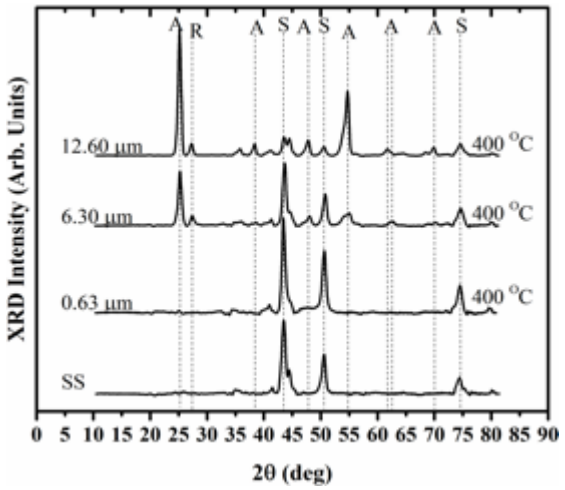

Figure 10 XRD spectra of coatings with varying thicknesses deposited at 400 °C. A = anatase, R = rutile, S = austenitic stainless steel.

The stainless steel substrate XRD peaks (labelled S) appear at 43°, 51° and 75° [34]. Anatase peaks (labeled A) for diffraction by (101), (004), (200), (211), (118) and (220)

planes appear at 25°, 38°, 48°, 55° , 62° and 70°, respectively [35, 36, 37]. Rutile TiO_2 planes (110), (101) and (211) diffract at 27°, 36° and 55°, respectively (labeled R) [38]. Only the two thicker coating samples had detectable peaks emanating from the coating. The weight fraction of rutile (W_R) was determined by [39]:

$$W_R = \frac{I_R}{0.886I_A + I_R}$$

Where I_R and I_A are the integrated intensity of the (110) rutile peak and the (101) anatase peak respectively. The mass fraction of the rutile phase was 17% for the 6.3 μm film and 10% for the 12.6 μm coating. According to reference [20] nucleation of this phase slows down after a complete surface coverage (100 nm) is attained paving the way for the nucleation of the anatase phase. As the anatase phase gets thicker the level of interaction between the buried rutile phase and the scattering beam deteriorates. The substrate to coating intensity ratio is in agreement with the photocalytic performance of these films.

3.3 Photocatalytic Activity The results of the photocatalytic activity study of TiO_2 coatings on SS are plotted in Figures 11 and 12. Figure 11 shows the dependence of photo-bleaching time on the thickness of the TiO_2 coatings deposited at 400 °C.

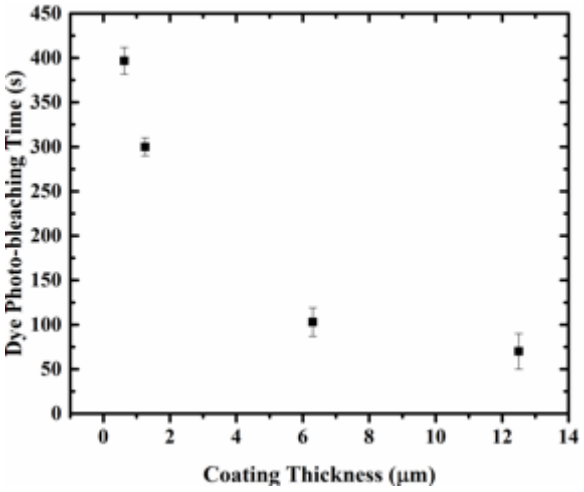

Figure 11 The photo-bleaching time as a function of thickness of TiO_2 coatings deposited on SS at 400 °C . Error bars are standard deviation over three experiments.

The decreased photo-bleaching time is an indication of increasing photocatalytic activity. The thicker coatings have the shortest photo-bleaching time, with the fastest bleaching in 75 seconds. This improved PC activity with increasing coating thickness has also been reported by Tada and Tanaka [21] for sol-gel deposited TiO_2 on quartz substrates and Duminica et al. [20] for atmospheric pressure MOCVD TiO_2 on stainless steel. This could either mean a diffusion of the Fe^{3+} cations from the substrate into the coating or an imperfect lattice around the substrate/film interface. The diffusion of Fe^{3+} cations from the substrate into the coating favours nucleation of the less desirable rutile phase, which then stops after the entire deposition surface is covered. The imperfect interface leads to the scattering of photoexcited carriers and enhances recombination reducing the probability of carriers reaching the surface and being used for redox reactions [21]. A lower photocatalytic activity for thinner films should also be expected due to enhanced influence of the imperfect interface.

Figure 12 shows the dependence of the photo-bleaching time on the deposition temperature of the coatings.

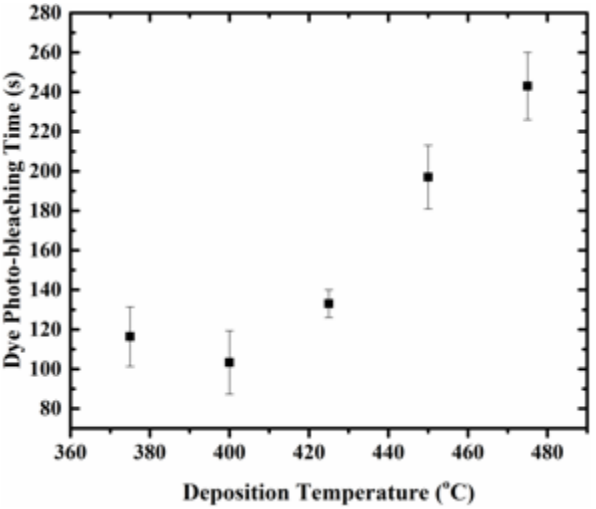

Figure 12 The photobleaching time as a function of the deposition temperature for ≈ 6.00 μm TiO_2 coatings deposited on stainless steel. Error bars are standard deviation over three experiments.

The dependence of photo-bleaching time on the deposition temperature exhibits a trend similar to that observed for the crystallite size. The highest temperature coating (475 °C), had the largest crystallite size (see Figure 7), and yielded the least active coating. A comparison between crystallite size and time to bleach, Figure 13, shows an increasing trend. The temperature of 400 °C which gave the smallest crystallite size yielded the most active coating as reported in [21]. The shortest photo-bleaching time gives an RZ ink reduction rate (≈ 0.0125 s^{-1}), which is much higher than the highest reduction rate reported by Zita et al. [39] for TiO_2 coatings deposited on glass substrate with a SiO_2 pre-coating by sol-gel method. The photo-bleaching times for the 12.6 μm thick coatings deposited at 400 °C have been compared to those of commercial self-cleaning glass. The coatings were found to be several times shorter than those commercial self-cleaning coatings [40].

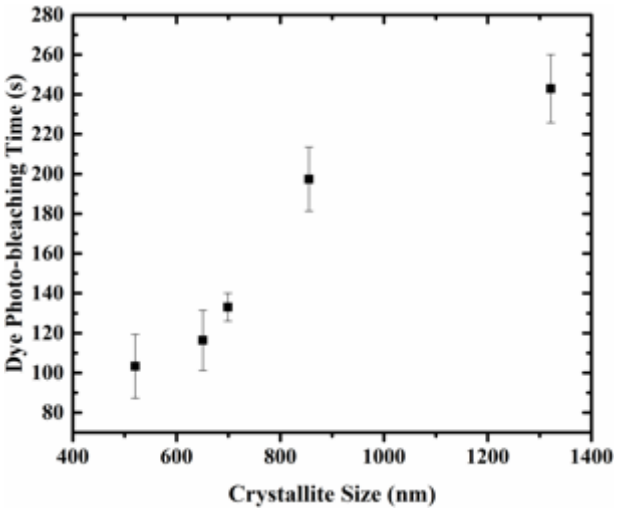

Figure 13 The photo-bleaching time as a function of crystallite size

3.3 Coated touch surface objects Figure 14 illustrates a chrome-covered brass door handle before and after coating with a nominally 10 μm thick titania film. Prior to the deposition, the handle was degreased with ethanol and ultrasonically cleaned with a water and detergent solution.

The part was placed in the chamber such that the surface areas that would be exposed to human contact under normal working conditions were open to the precursor vapour. The handle was heated using RF induction with a coil geometry specifically designed to provide uniform heating. The deposition was performed at a temperature of 400°C for 1000 pulses. The deposition conditions were the same as the 12.6 μm coating condition on the SS samples, so the coating is expected to be at least 10 μm thick.

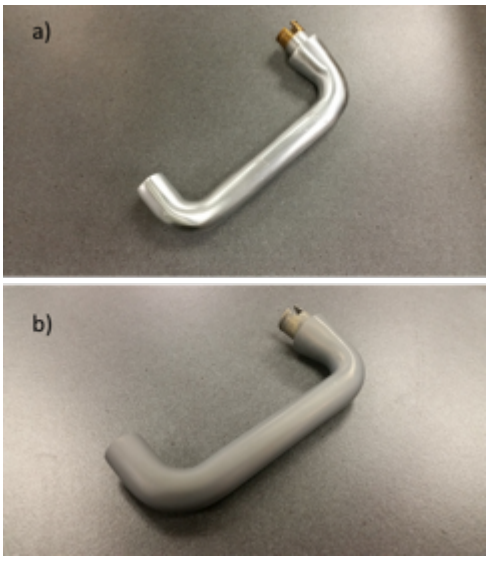

Figure 14 Chrome-coated brass door handle a) prior to deposition and b) after a uniform, thick (more 10 μm) coating of TiO_2 was deposited.

The thick TiO_2 coating appeared to have a uniform shade of grey and no delamination was observed. The observations suggest that uniform heating was obtained and that the coating thickness is reasonably uniform. The coated handle was placed in a pressure cooker with steam at 2 bar for 20 minutes with no observable effect on the coating.

4 Conclusions The pulsed-pressure MOCVD process was used to deposit titania films from TTIP solution on stainless steel. Growth rate, thickness and morphology were studied for coatings deposited at 400 ^{o}C with thicknesses varying between 0.17 μm and 12.6 μm being achieved by varying the number of pulses and therefore the deposition time. A set of films were deposited over a temperature range 375 ^{o}C to 475 ^{o}C using approximately 300 pulses (40 minutes) and producing nominally 6 μm thick films. XRD and EDS confirmed near-stoichiometric mixed anatase and rutile titania in the 6.3 and 12.6 μm films deposited at 400 ^{o}C. The films were all slightly oxygen difficient. The amount of iron in the films increased with deposition temperature due to interdiffusion from the substrate, but was less than 0.6 atomic percent at 400 ^{o}C. The photocatalytic activity was highest for the 6.3 μm film grown at 400 ^{o}C, which also had the smallest crystallite size of approximately 500 nm (largest specific surface area).

The scaled-up pp-MOCVD reactor was used to coat a typical hospital door handle with a uniform coating of TiO_2 with at least 10 μm thickness. Future work includes adhesion, scratch and wear testing, and testing of the bacterial loading of coated handles compared to uncoated handles in a hospital ward.

Acknowledgements The authors acknowledge funding from KOTI Technologies. The authors are grateful to Mr Mike Flaws for assistance with SEM work and Mr Matthew Polson for assistance with XRD.

References

[1] L. Warren, R. Sanborn, Am. J. Public Health Nations Health, **53**, 1278-1283 (1963).
[2] NOA The management of Hospital Acquired Infection in Acute NHS Trusts in England (2000).
[3] A. M. Emmerson, J. E. Enstone, M. Griffin, M. C. Kelsey, E. T. M. Smyth, J. of Hospital Infection, **32,** 175-190 (1996).
[4] S. Dancer, The Lancet Infectious Diseases, **8,** 101-108 (2008).
[5] J. M. Boyce, J. of Hospital Infection, **70,** 2-7 (2008).

[6] K. Page, M. Wilson, I. P. Parkin, J. of Materials *Chemistry,* **19,** 3819-3831 (2009).
[7] H. Lara, N.V. Ayala-Nunez, L.Turrent, C.R. Padilla, World J. Microbiol. Biotechnol., **26**, 615-621 (2010).
[8] B. Despax, C. Saulou, P. Raynaud, L. Datas, M. Mercier-Bonin, Nanotechnology, **22**, 175101 (2011).
[9] K. Sheehy, A. Casey, A. Murphy, A. Chambers, J. Colloid Interface Sc., **443**, 56-64 (2015).
[10] G. E. Schaumann, A. Philippe, M. Bundschuh, G. Metreveli, S. Klitzke, D. Rakcheev, A. Grün, S. K. Kumahor, M. Kühn, T. Baumann, F. Lang, W. Manz, R. Schulz, H.-J. Vogel, Sci. Total Environ. (2014) in Press.
[11] M. Pelaez, N. T. Nolan, S. C. Pillay, M. K. Seery, P. Falaras, A. G. Kontos, P. S. Dunlop, J. W. J. Hamilton J. A. Byrne, K. O'shea, M. H. Entezari, D. D. Dinysiou, Appl. Catal. B: Environmenta, **125,** 331-349 (2012).
[12] A. Di Paola, E. Garcia-Lopez, S. Ikeda, G. Marci, B. Ohtani, L. Pamisano, Catal. Today, **75,** 87-93 (2002).
[13] H. Zhang, J. F. Banfield, J. Phys. Chem. B, **104,** 3481-3487 (2000).
[14] E. Bannier, G. Darut, E. Sánchez, A. Denoirjean, M.C. Bordes, M.D. Salvador, E. Rayón, H. Ageorges, Surf. Coat. & Technol. **206**, 142-150 (2013).
[15] K. Midtdal, B. P. Jelle, Solar energy Matr. & Solar Cells, **109**, 126-141, (2013).
[16] T. Luttrell, S. Halpegamage, J. Tao, A. Kramer, E. Sutter, M. Batzill, Sci. Rep. **4**, 4043 (2014).[18] D. A.
[17] H. Hanaor, C. C. Sorrell, J Mater Sci **46**, 855–874 (2011).
[18] M. D. Hernandez-Alonso, F. Fresno, S. Suarez and J. M. Coronado, Energy Environ. Sci., **2**, 1231-1257 (2009).
[19] Z. Zhang, C.-C. Wang, R. Zakaria, J. Y. Ying, J. Phys. Chem. B **102**, 10871-10878 (1998).
[20] F.-D. Duminica, F. Maury, R. Hausbrand, Surf. Coat. Technol., **201**, 9304-9308 (2007).
[21] H. Tada, M. Tanaka, Langmuir, **13**, 360-364 (1997).
[22] S. Krumdieck, J. Aust. Ceram. Soc., 48 69-79 (2012).
[23] S. P Krumdieck,., H. M. Cave, S. Baluti, M. Jermy, A. Peled, Chem. Eng. Sci., **62** 6121-6128 (2007)
[24] H. M. Cave, S. P. Krumdieck, M. C. Jermy, Chem. Eng. J.,**135,** 1-2, 120-128 (2008).
[25] D. Lee, S. Krumdieck, S. Davies Talwar, Surf. Coat. Technol., **230**, 39-45 (2013).
[26] V. Siriwongrungson, S. Krumdieck, Chem. Vap. Deposition, **17,** 1-11 (2011).
[27] A. Mills, J. Hepburn, D. Hazafy, C. O'Rourke, J. Krysa, M. Baudys, M. Zlamal, H. Bartkova, C. E. Hill, K. R. Winn, M. E. Simonsen, E. G. Søgaard, S. C. Pillai, N. S. Leyland, R. Fagan, F. Neumann, C. Lampe, T. Graumann, J. Photochem. Photobiol. A: Chem 272, 18-20 (2013).
[28] http://www.iphotocat.com/tests/rz-test/rz-dye-photocatalytic-activity-test/
[29] P. Kajitvichyanukula, P. Amornchat Sci. Technol. Adv. Mater. 6, 344-347 (2005).
[30] R. E. Chin, Ceramography: Preparation and Analysis of Ceramic Microstructures (ASM International, Ohio, 2002), p. 149.
[31] H.-E. Cheng, C.-C. Chen, J. Electrochem. Soc., **159**, D604-D607 (2008).
[32] M.-K. Lee, J.-J. Huang, T.-S. Wu, Semicond. Sci. Technol. **20**, 519-523 (005).
[33] J. A. Van Orman, K. L. Crispin, Rev Mineral Geochem, **72**, 757-825 (2010).
[34] G. Yildirim, S. Bal, M. Gulen, A. Varilci, E. Budak, and M. Akdogan, Cryst. Res. Technol. **47**, 195 – 201 (2012).
[35] Z. Antic, R. M. Krsmanovic, M. G. Nikolic, M. Cincovic, M. Mitric, S. Polizzi, M. D. Dramicanin, Mat. Chem. Phys., **135**, 1064-106 (2012).
[36] K. Thamaphat, P.Limsuwan and B. Ngotawornchai, J. Kasetsart Nat. Sci., **42**, 357 - 361 (2008)
[37] Snejana Bakardjieva, Vaclav Stengl, Lorant Szatmary, Jan Subrt, Jozef Lukac, Nataliya Murafa, Daniel Niznansky, Karel Cizek, Jaromir Jirkovsky and Nadia Petrova, J. Mater. Chem. 16, 1709-1716 (2006)
[38] A. Fujishima, X. Zhangb, D. A. Tryk, Surf. Sci. Rep., **63**, 515582 (2008).
[39] J. Zita, J. Kry´ s, U. C˘ernigoj, U.L.-S˘tangar, J.Jirkovsky´, J.Rathousky, Catal. Today **161**, 29-34 (2011).
[40] A. Mill, D. Keir, "Report on assessing photocatalytic activity by colour changing inks using an INTEC method", QUEENS IPS, (2014).